ADVANCED MATERIALS
www.advmat.de

Reliable and Remote Monitoring of Absolute Temperature during Liver Inflammation via Luminescence-Lifetime-Based Nanothermometry

Yingli Shen, José Lifante, Irene Zabala-Gutierrez, María de la Fuente-Fernández, Miriam Granado, Nuria Fernández, Jorge Rubio-Retama, Daniel Jaque, Riccardo Marin, Erving Ximendes, and Antonio Benayas**

Temperature of tissues and organs is one of the first parameters affected by physiological and pathological processes, such as metabolic activity, acute trauma, or infection-induced inflammation. Therefore, the onset and development of these processes can be detected by monitoring deviations from basal temperature. To accomplish this, minimally invasive, reliable, and accurate measurement of the absolute temperature of internal organs is required. Luminescence nanothermometry is the ideal technology for meeting these requirements. Although this technique has lately undergone remarkable developments, its reliability is being questioned due to spectral distortions caused by biological tissues. In this work, how the use of bright Ag_2S nanoparticles featuring temperature-dependent fluorescence lifetime enables reliable and accurate measurement of the absolute temperature of the liver in mice subjected to lipopolysaccharide-induced inflammation is demonstrated. Beyond the remarkable thermal sensitivity (≈ 3% $°C^{-1}$ around 37 °C) and thermal resolution obtained (smaller than 0.3 °C), the results included in this work set a blueprint for the development of new diagnostic procedures based on the use of intracorporeal temperature as a physiological indicator.

1. Introduction

For centuries mankind has been aware of the intrinsic relationship between temperature and health. Fever (increased body temperature in the face of infectious or inflammatory processes) is the most glaring example. The temperature of a given organ is a consequence of the delicate balance between several factors including external temperature, metabolic activity, and blood perfusion.[1] As a result, minimal alterations in those parameters can result in a change in the temperature of an organ. As such, temperature fluctuations can be used as an early indicator of the development of diseases. The temperature–illness link has been reported for numerous maladies with disruptive effect on the society, such as degenerative processes of the nervous system, acute inflammation caused by infectious agents, and cardiovascular diseases.[2] An especially striking cause of both body and internal organs temperature elevation is systemic inflammation, which is a severe condition with a high rate of morbidity and mortality.[3] Hence, thermal monitoring of tissues and organs has emerged as a valuable tool for early detection of threatening diseases.[3,4] To be effective, thermal monitoring should be achieved remotely, without perturbing the temperature of the tissue while measuring, also avoiding physical alterations of the organ under investigation.

Unfortunately, most conventional thermal-sensing technologies are invasive—as they require the insertion of microscopic thermal sensors like thermocouples—while noninvasive thermal imaging by infrared cameras only allows measurement of surface temperature.[5] In this context, luminescence thermometry represents an alternative technique that overcomes these limitations. It is based on the use of luminescent nanothermometers (LNThs) as remote thermal reporters.[6,7] LNThs are nanoparticles (NPs), proteins, or dyes whose luminescence is strongly temperature-dependent. Originally proposed for intracellular temperature measurement,[8,9] LNThs have been later applied for remote thermal sensing in animal models.[10] In such models, the use of LNTh has enabled, for

Y. Shen, J. Lifante, M. de la Fuente-Fernández, M. Granado, N. Fernández, D. Jaque, R. Marin, E. Ximendes, A. Benayas
Nanomaterials for Bioimaging Group (NanoBIG)
Universidad Autónoma de Madrid
Madrid 28049, Spain
E-mail: erving.ximendes@uam.es; antonio.benayas@uam.es

J. Lifante, N. Fernández, D. Jaque, E. Ximendes, A. Benayas
Nanomaterials for Bioimaging Group (NanoBIG)
Instituto Ramón y Cajal de Investigación Sanitaria
Ctra de Colmenar Viejo Km 9,100, Madrid 28034, Spain

I. Zabala-Gutierrez, J. Rubio-Retama
Departamento de Química en Ciencias Farmacéuticas
Facultad de Farmacia
Universidad Complutense de Madrid
Plaza Ramón y Cajal S/N, Madrid 28040, Spain

The ORCID identification number(s) for the author(s) of this article can be found under https://doi.org/10.1002/adma.202107764.

DOI: 10.1002/adma.202107764

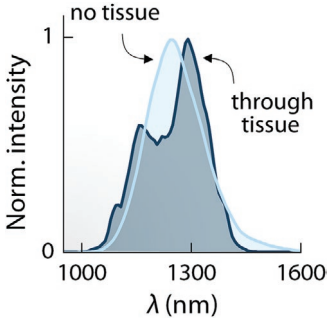

Figure 1. Emission spectra of Ag_2S NPs obtained in the absence and presence of tissues revealing the broad emission band within the second biological window and how it is distorted by the wavelength-dependent extinction of tissues. The emission spectra obtained in the presence of tissues were obtained in in vivo conditions. Data were extracted from ref. [16].

example, noninvasive monitoring of brain activity,[11] diagnosis of ischemic tissues,[12] detection of inflammation processes, and control of thermal therapies of solid tumors.[13,14] Despite these promising demonstrations, in vivo luminescence thermometry is still not a completely reliable technique. Not only the presence of biological tissues in the optical path significantly reduces the amount of detected luminescence;[7,15,16] more importantly, they induce spectral distortions that yield inaccurate thermal readouts.[17] The use of LNThs operating in the infrared biological windows (where tissues are partially transparent) minimizes these issues to some extent. However, tissue-induced spectral distortions still occur in the infrared spectral range (see **Figure 1**) and indeed lead to erroneous thermal readouts.[15] Although it has recently been shown that a rational analysis of spectra can (in some very specific cases) increase the reliability of thermal measurements,[13] alternative measuring approaches should be adopted to achieve fully reliable thermal reading.

Fluorescence lifetime (τ) is traditionally thought not to be affected by photon-tissue interaction. Indeed, lifetime-based LNThs (τ-LNThs, NPs with a strongly temperature-dependent lifetime) have recently been proposed as reliable thermal reporters. To that end, τ-LNThs based on lanthanide-doped NPs have been used for reliable subcutaneous in vivo thermal sensing.[18] However, the low brightness of these species (due to their low molar absorption coefficient) cripples their use in thermal monitoring of internal organs. Ag_2S NPs, instead, appear to be better suited as τ-LNThs for in vivo applications due to a unique combination of properties: low toxicity, high brightness, temperature-dependent lifetime around 37 °C, and spectral operation in the second biological window (NIR-II, 1000–1400 nm).[19,20] As a consequence, it has been used for several biomedical studies.[21] Nevertheless, to this date, absolute thermal monitoring of an internal organ using Ag_2S NPs or any other LNTh has not been demonstrated.

In this work, the robustness of Ag_2S NPs as τ-LNThs was initially evaluated through ex vivo experiments and simple numerical calculations. After ascertaining the negligible impact of tissue extinction coefficient in the lifetime-based thermal readout, the actual potential of Ag_2S NPs as τ-LNThs for thermal monitoring of internal organs, in our case the liver, was demonstrated in an in vivo inflammation model.

2. Results and Discussion

Figure 2A shows a representative transmission electron microscopy (TEM) image of the Ag_2S NPs used in this work. Ag_2S NPs were synthetized via a thermal decomposition process followed by a sonochemical post-synthesis treatment that improves the quality of the NP surface and, as a result, their spectroscopic properties. Details about the synthesis procedure are given in the Experimental Section. The resulting NPs were rendered water-dispersible via modification of their surface with poly(ethylene glycol) (PEG). The average size of the final PEGylated Ag_2S NPs was (9 ± 1) nm (Figure 2B) and their hydrodynamic size in aqueous solutions was measured to be 21 ± 3 nm (see Figure S1, Supporting Information). These Ag_2S NPs show excellent colloidal stability in phosphate buffer saline (PBS 1x) without sign of precipitation during weeks. In addition, the Ag_2S NPs demonstrated to be quite stable in colloidal dispersion under temperature variation within the 20–50 °C range (Figure S2, Supporting Information). Figure 2C shows an optical image of colloidal dispersions of Ag_2S NPs and commercial Ag_2S NPs (Sinano Int., hereafter c-Ag_2S NPs) in PBS 1x both at a concentration of 0.5 mg mL^{-1}. While both dispersions were transparent and homogeneous with no evidence of cluster formation, when optically excited with 800 nm radiation, our Ag_2S NPs showed a much stronger infrared signal centered at 1250 nm. Indeed, the fluorescence quantum yield (QY, defined as the fraction of absorbed photons that are converted into emitted photons) of the here developed Ag_2S was experimentally determined to be 2.3%. This value yields a brightness $B = \varepsilon \times \mathrm{QY}$ ($\varepsilon = 8 \times 10^4$ M^{-1} cm^{-1} being the molar absorption coefficient of the Ag_2S NPs at 800 nm) close to 1.8×10^3 M^{-1} cm^{-1}. This value is almost 20-fold larger than the brightness of the only other system that has been previously used for in vivo lifetime thermal sensing, i.e., lanthanide-doped NPs with brightness typically around 10^2 M^{-1} cm^{-1} (see **Table 1**). This higher brightness is mirrored by a longer fluorescence lifetime compared to c-Ag_2S NPs, as evidenced in Figure 2D. To evaluate the performance of Ag_2S NPs as τ-LNThs, a systematic study of the thermal dependence of their intrinsic fluorescence lifetime was carried out. Figure 2E includes the fluorescence decay curves corresponding to a colloidal dispersion of Ag_2S NPs obtained at different temperatures within the physiological range (20–50 °C). As it can be observed in Figure 2F, the average fluorescence lifetime ($\tau = \frac{\int I(t)t\mathrm{d}t}{\int I(t)\mathrm{d}t}$, where $I(t)$ is the emitted intensity at time t after laser excitation) follows a monotonic decrease with temperature. This temperature-induced lifetime shortening is in accordance with previous works dealing with Ag_2S NPs synthetized by other methods.[20] This observation suggests that this is an intrinsic property of Ag_2S as a material. A closer analysis of the experimental data of Figure 2F reveals that the fluorescence lifetime shortens at a rate of $\frac{1}{\tau}\frac{\mathrm{d}\tau}{\mathrm{d}T} \approx 3\%$ $°C^{-1}$ around 37 °C (see Figure S4b, Supporting Information). According to the data inserted in Table 1, this value is among the largest relative thermal sensitivities (S_r) reported for τ-LNThs.

When proposing a thermal probe for in vivo applications, reporting its sensitivity is not enough to determine its robustness and reliability. It is also necessary to determine

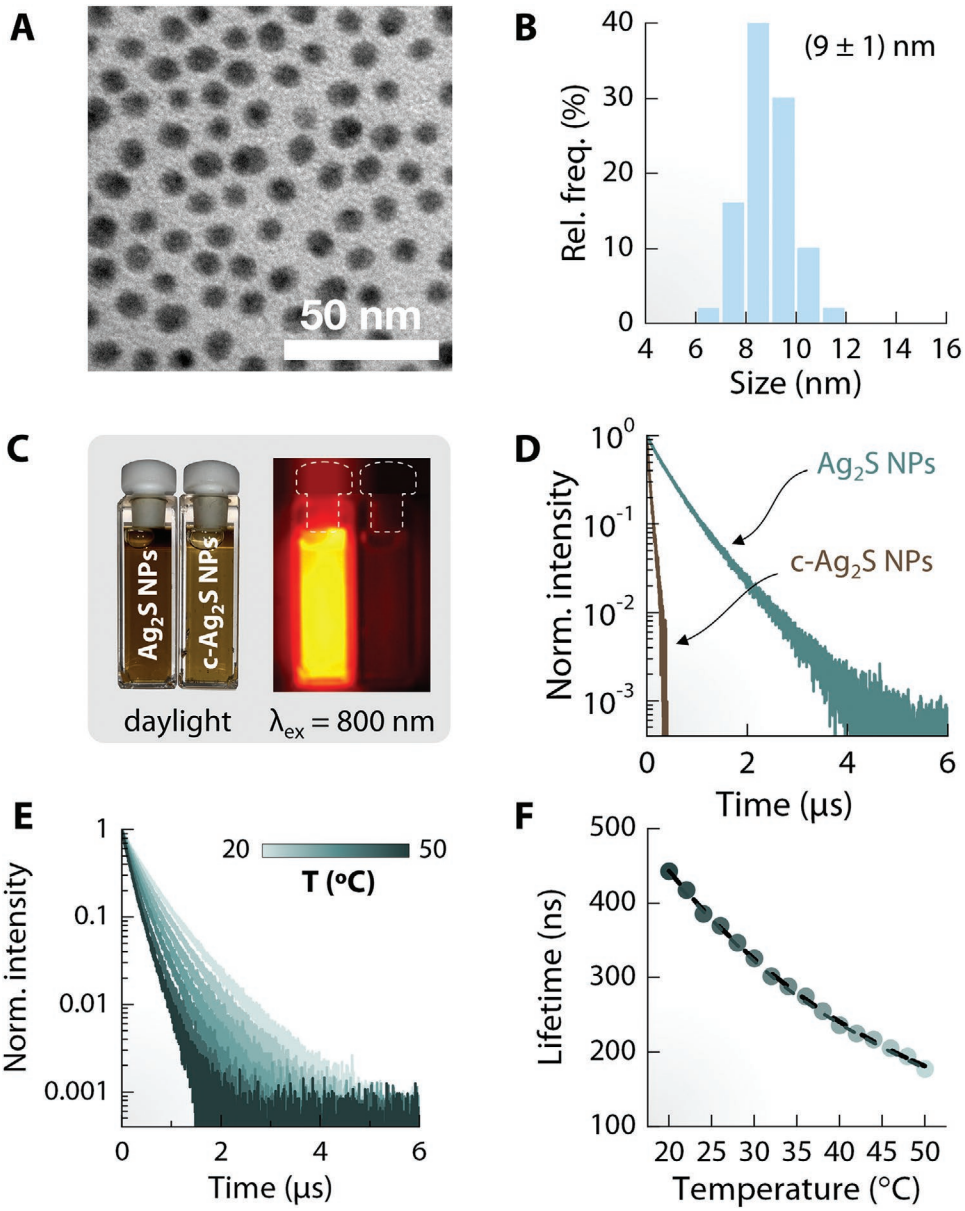

Figure 2. Characterization of Ag_2S τ-LNThs. A) Characteristic TEM image of PEGylated Ag_2S NPs used in this study. B) Size histogram revealing an average particle size of (9 ± 1) nm as measured by TEM. C) Optical and infrared images of colloidal dispersion of Ag_2S and c-Ag_2S NPs in PBS 1x at a concentration of 0.5 mg mL^{-1}. D) Fluorescence decay curves for synthesized (teal) and commercially available (brown) Ag_2S NPs obtained with excitation and emission wavelengths of 800 and 1200 nm, respectively. E) Fluorescence decay curves of Ag_2S NPs obtained at different temperatures ranging from 20 to 50 °C. F) Temperature dependence of the average lifetime of Ag_2S NPs determined from the analysis of the decay curves included in (E).

whether the sensor is affected by thermal hysteresis and/or by the medium in which it is inserted. A simple way by which one could evaluate the former possibility is through the verification of the stability of the thermal sensors after consecutive heating and cooling cycles. **Figure 3**A presents the fluorescence lifetime of Ag_2S NPs as obtained during different heating and cooling cycles from 25 up to 45 °C. Lifetime values at both temperatures were not affected by previous thermal cycles revealing the absence of any thermal memory within the physiological range. To that end, a repeatability of 0.99 was calculated for the proposed thermometric approach (see the Supporting Information). The effect of the medium, on the other hand, can be evaluated through the experiment depicted in Figure 3B. Briefly, the Ag_2S NPs were optically excited by a 10 ns pulsed laser operating at 800 nm. The fluorescence time decay curve was then registered with an infrared photomultiplier. To mimic the conditions generally found in in vivo experiments, a cuvette of variable thickness filled with a dispersion of intralipid (meant to reproduce the light-attenuation properties of tissues in NIR-II) was placed within the optical path of detection.[25] At this point, the presence of two possible artifacts could be evaluated: i) tissue-induced changes in the measured value of

Table 1. Comparison of lifetime-based luminescent nanothermometers. Optical properties of the most representative systems used for fluorescence lifetime-based thermal sensing.

System	λ_{exc} [nm]	λ_{em} [nm]	τ	QY [%]	ε [M^{-1} cm^{-1}]	B [M^{-1} cm^{-1}]	S_r [% C^{-1}]	Used in vivo?	Ref.
Carbon dots	355	421	9.4 ns	5	6.6 10^4	3300	0.006	No	[22]
CdTe QDs	580	654	32 ns	31	3.4 10^5	105 400	0.0045	No	[23]
$NaYF_4$:Yb,Nd	808	1000	420 µs	1.77	1.3×10^4	221	0.93	No	[24]
Ag_2S NPs	808	1200	35 ns	0.08	4.6×10^5	368	3.5	No	[20]
Polymer	450	564	7 ns	0.3	1.7×10^6	5220	0.29	No	[9]
$NaYF_4$:Yb^{3+}, Nd^{3+} @CaF_2	800	1000	625 µs	N/A	N/A	N/A	1.1-1.4	Yes	[18]
Ag_2S NPs	808	1200	286 ns	2.3	4.5×10^5	10 350	3	Yes	This work

the fluorescence lifetime, and/or ii) tissue-induced changes in the thermal sensitivity of the fluorescence lifetime. While the former does not depend on the temperature of the tissue (intralipid in our case), the latter does, and only takes place when the optical properties of this medium are thermally dependent. To account for the effect of tissue temperature in the thermal sensitivity of our Ag_2S NPs, a second configuration of the experiment was added to the set-up. In it, instead of changing the temperature of Ag_2S NPs (through the action of heating plate in position 1, Figure 3B), it is the temperature of the cuvette with intralipid which is varied (heating plate in position 2, Figure 3B) while keeping its thickness fixed.

The results obtained under the first configuration (Figure 3C) reveal that the absolute value of the fluorescence lifetime of Ag_2S NPs, under different temperatures, is not affected by the presence of a tissue (thickness up to 4 mm) at a constant temperature (20 °C). This result is quite remarkable because, despite this independence at the lifetime level, tissue-induced light attenuation causes a marked reduction of the detected intensity (see Figure S5, Supporting Information). Therefore, Figure 3C demonstrates the superiority of fluorescence lifetime as a thermometric parameter over other parameters obtained from the spectral domain. The data also agrees with the results recently published by M. Tan and co-workers, who also demonstrated the robustness of sub-tissue lifetime nanothermometry with lanthanide-doped NPs.[18] The results obtained with the second configuration (Figure 3D) reveal that, within the experimental error, the temperature of the tissue does not affect the measured fluorescence lifetime. The data are, again, supportive of the advantage of using fluorescence lifetime instead of other parameters obtained through the analysis of the luminescence spectrum.[15] Finally, the systematic error on the lifetime measurement (caused by detector noise, electronics, pulse-to-pulse fluctuations, and analysis procedure) was also estimated by performing consecutive signal acquisitions while keeping the experimental parameters constant. These results are included in Figure 3E, and they reveal a relative systematic error of 1%. Considering an average thermal sensitivity of 3% $°C^{-1}$, this systematic error leads to an error in the thermal readout of 0.3 °C.

While the presence of both thermal hysteresis and tissue-induced artifacts was discarded, the uncertainty in lifetime-based thermal readouts caused by tissue-induced photon scattering needed be estimated. Due to tissue-induced scattering, the trajectory of photons deviates from a purely ballistic one (Figure 3F). If the direction of a photon is perpendicular to the surface of a tissue, its average path length, $\langle L\rangle$, is given by[26]

$$\langle L\rangle = \frac{\sqrt{3\mu_s'}}{2\sqrt{\mu_a}} \frac{l^2\sqrt{3\mu_s'\mu_a}}{l\sqrt{3\mu_s'\mu_a}+1} \quad (1)$$

where l, μ_s', and μ_a are the thickness, the reduced scattering coefficient and the absorption coefficient of the tissue. Since $\langle L\rangle > l$, it takes more time for the scattered photons to cross the tissue than the ones undergoing ballistic trajectories. This time delay, $\delta\tau$, causes an enlargement in the detected fluorescence lifetime that can be calculated as follows

$$\delta\tau = \left(\langle L\rangle - l\right)\frac{n}{c} = \frac{n}{c}l\left(\frac{3l}{2}\frac{\mu_s'}{l\sqrt{3\mu_s'\mu_a}+1} - 1\right) \quad (2)$$

where $n \approx 1.4$ is the refractive index of tissue and c is the speed of light in vacuum.[27] The existence of this tissue-induced fluorescence lifetime enlargement leads to a discrepancy between the actual sub-tissue temperature and the one obtained translating the measured lifetime into temperature through the calibration curve. This tissue-induced temperature uncertainty, δT_{tissue}, can be written as

$$\delta T_{tissue} = \left(\frac{dT}{d\tau}\right)\delta\tau = \frac{dT}{d\tau}\frac{n}{c}l\left(\frac{3l}{2}\frac{\mu_s'}{l\sqrt{3\mu_s'\mu_a}+1} - 1\right) \quad (3)$$

where $d\tau/dT$ is the rate at which the fluorescence lifetime varies with temperature. At 37 °C, this rate is close to –9 ns $°C^{-1}$ (see Figure S4a, Supporting Information). Figure 3G shows the thickness dependence of $\delta\tau$ and δT_{tissue} as calculated from Equations (2) and (3) and by assuming classical values reported for absorption and scattering coefficients of tissues in the near-infrared (NIR) (μ_s' = 9 cm^{-1} and μ_a = 1 cm^{-1} at 1200 nm).[27] As it can be observed, tissue-induced optical extinction induces both a fluorescence lifetime enlargement and a systematic error in temperature determination that, in both cases, increases with the tissue thickness. Note that, even for the largest tissue thickness here considered (5 cm), the tissue-induced fluorescence lifetime enlargement (0.6 ns) is more than two orders of magnitude smaller than the lifetime of our Ag_2S NPs (250 ns at 37 °C). This enlargement leads, for a tissue thickness of 5 cm, to a temperature uncertainty of δT_{tissue} = 0.1 °C. The magnitude of this error is much lower than the ones obtained when extracting temperature from the spectral analysis of the emission of Ag_2S NPs (typically

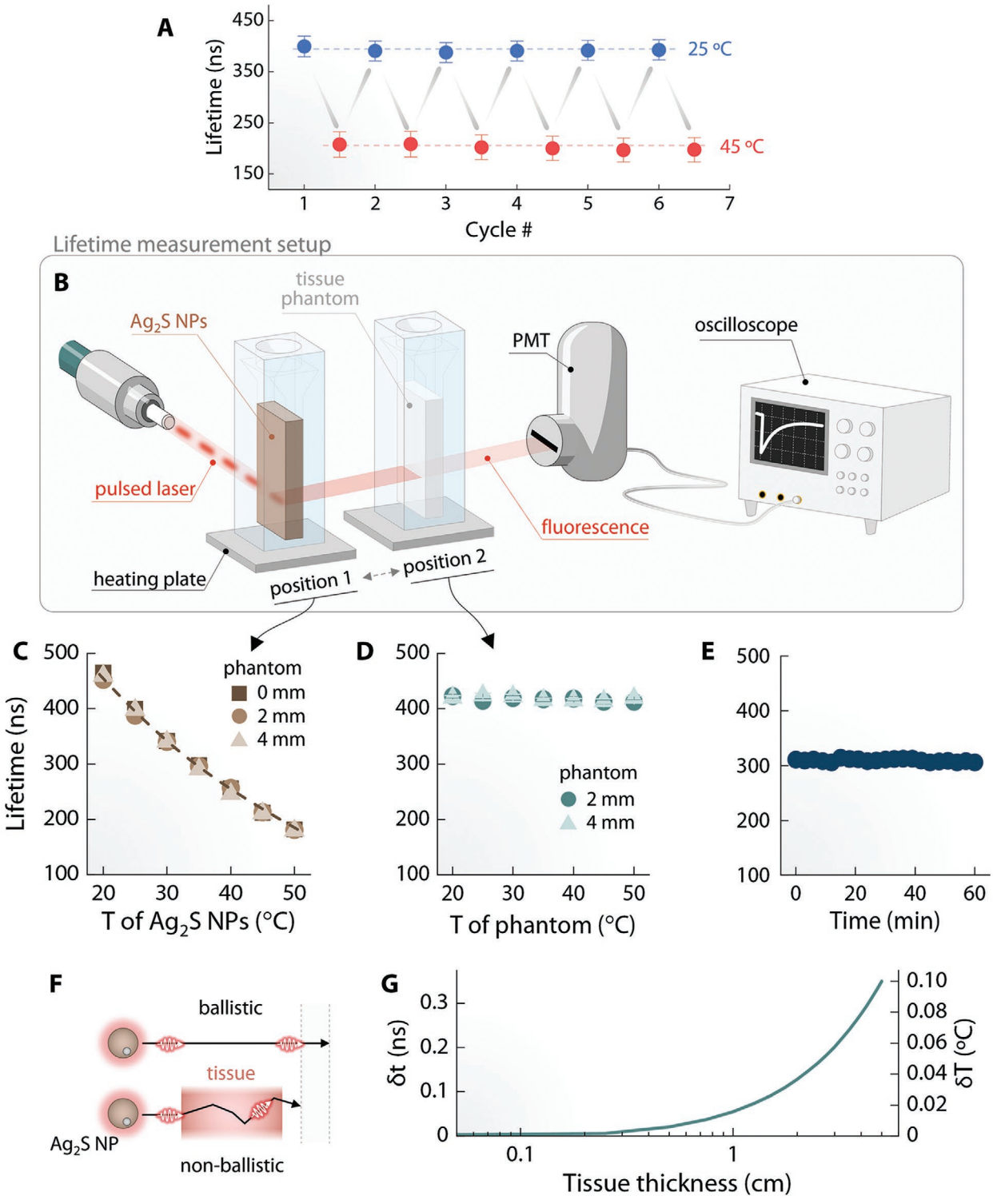

Figure 3. Robustness and reliability of Ag_2S NPs for lifetime-based sub-tissue thermal sensing. A) Fluorescence lifetime of Ag_2S NPs at 25 and 45 °C as obtained after consecutive heating and cooling cycles. B) Schematic representation of the experimental set-up developed to elucidate the influence of tissue thickness and temperature on the measured fluorescence lifetime of Ag_2S NPs. C) Temperature dependence of the fluorescence lifetime of Ag_2S NPs obtained for different tissue thicknesses. D) Fluorescence lifetime of Ag_2S NPs as a function of tissue temperature obtained for two tissue thicknesses. E) Fluorescence lifetime obtained in consecutive measurements to evaluate our systematic error in determining the fluorescence lifetime. F) Scheme showing the comparison between the trajectory and overall travelled path by a ballistic and nonballistic photon (passing through a scattering tissue) emitted by a Ag_2S NP over the course of the same time interval. G) Tissue-induced photon delay ($\delta\tau$) and tissue-induced thermal uncertainty (δT) as a function of tissue thickness.

few degrees for tissues of few millimeters).[15] Therefore, albeit tissue-induced photon scattering constitutes a source of error in lifetime-based thermal sensing, its effect can be considered negligible in the conditions generally encountered in in vivo measurements (i.e., lifetimes >100 ns and tissue thickness < 1 cm).

After validating the robustness and reliability of Ag_2S NPs as τ-LNThs, we explored their potential for accurate thermal monitoring of internal organs at the pre-clinical level. Specifically, we designed an in vivo experiment wherein liver temperature was monitored. Liver was selected due to the efficient accumulation of PEGylated Ag_2S NPs that is typically observed to occur after intravenous injection.[28] Additionally, the slow clearance process allows experiments on long time scales (i.e., in the order of hours) to be performed.[28]

To induce a temperature variation in this organ, we administered LPS through intraperitoneal injection (10 mg kg^{-1}) as a model of acute inflammation.[29] The administration of LPS induces an increase in circulating and hepatic concentrations of cytokines and inflammatory mediators, as well as a rise in the intracorporeal temperature in a dose-dependent manner.[30]

This procedure is summarized in **Figure 4**A. Prior to LPS administration, an intravenous injection of a Ag_2S NPs dispersion in PBS (100 µL at a mass concentration of 0.5 mg mL^{-1}) was performed. This ensured the presence of the thermal reporters at the liver before and during the inflammatory process. After LPS injection, the existence of an effective inflammatory response was evidenced by the significant increment in the hepatic gene expression of several proinflammatory markers such as tumor necrosis factor-alpha (TNF-α), Interleukin-6 (IL-6), Interleukin-1β (IL-1β), and inducible nitric oxide synthase (iNOS) compared to control mice injected with saline (Figure 4B).

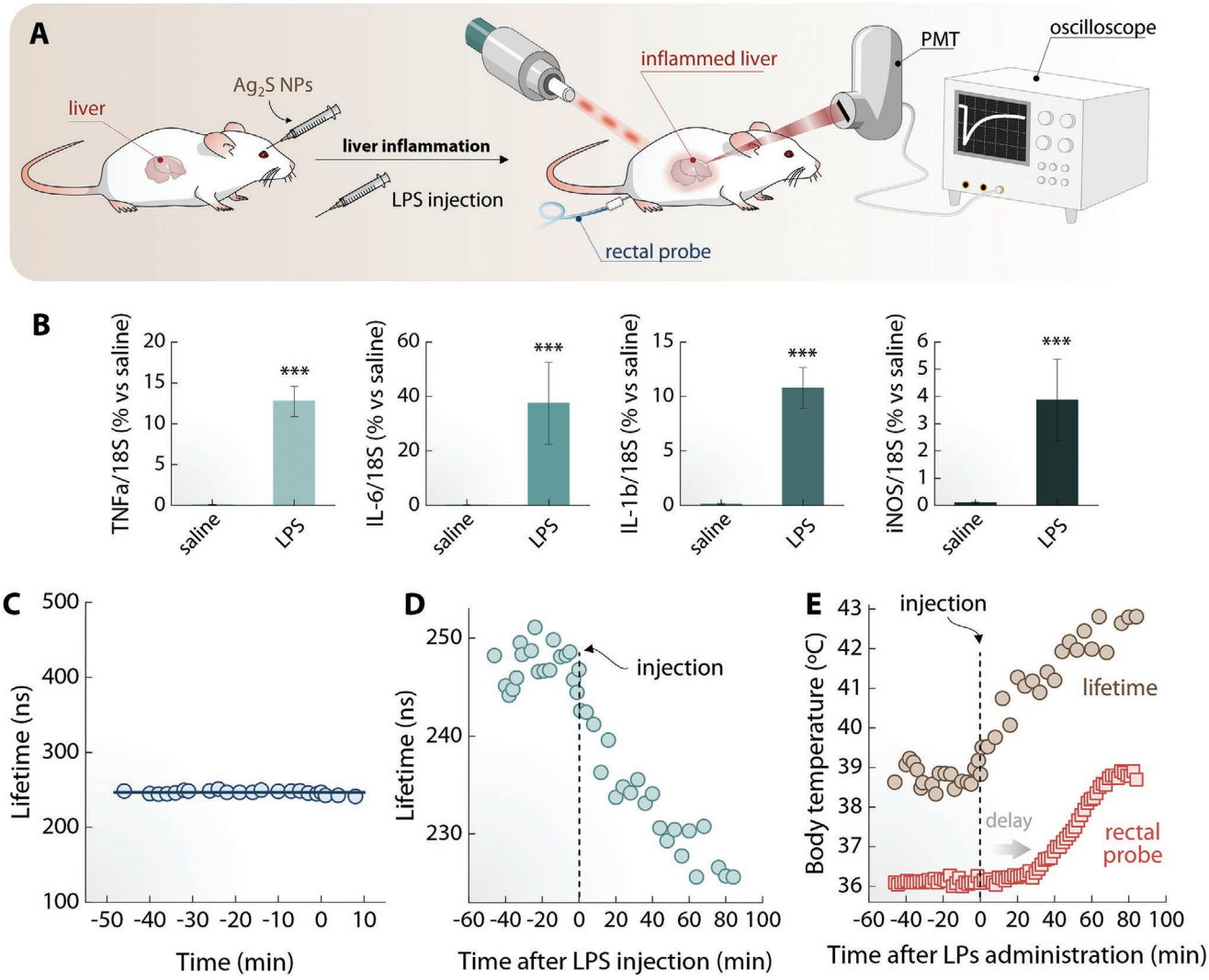

Figure 4. Real-time thermal monitoring of liver during inflammation. A) Schematic representation of the experimental procedure designed to monitor liver temperature during LPS-induced inflammation. B) Gene expression of proinflammatory markers (TNF-a, IL-6, IL-1b, and iNOS) in hepatic tissue after LPS injection. (*** Pv<v0.001 vs saline.) C) Time evolution of the fluorescence lifetime before LPS injection. The symbols are experimental data and the solid line indicates the average value over time. D) Time evolution of the fluorescence lifetime after LPS injection. E) Time evolution of liver temperature after LPS injection (brown circles) and rectal temperature (red squares).

Before induction of the inflammatory process, fluorescence decay curves of Ag_2S NPs were continuously acquired to determine the basal temperature and the thermal stability of the liver (Figure 4C). Details about the experimental set-up used for the acquisition of fluorescence decay curves in in vivo experiments are given in the Experimental Section. The fluorescence lifetime retrieved from the measurements oscillated around an average value of 239 ns (solid line in Figure 4C) with a standard deviation of ±2 ns. Data in Figure 4C, obtained using the calibration curve included in Figure 2F, reveals an average liver temperature close to 38.7 °C and a thermal readout fluctuation of ±0.3 °C. Given that exposure to pulsed radiation did not seem lead to appreciable temperature increase in the animal (Figure S6, Supporting Information), we treated this as the actual basal temperature of the organ. Note also that the observed thermal fluctuation matches the one estimated from the systematic error performed in lifetime measurement by our experimental setup (vide supra). It should be highlighted that the error provided by other LNThs systems reported in the literature and working in less challenging conditions (for instance, in more superficial tissues) always surpasses 0.5 °C.[17] The only notable exception is represented by the recent work of Maturi et al. wherein thermal uncertainties below 0.1 °C were reported for in vivo thermal reading of a superficial tumor.[31] Nonetheless, it should be underscored that such a low thermal error could only be achieved with an intense post-acquisition manipulation of the data through the use of multiple linear regression analysis.

After verifying that the liver temperature was stable, we administered intravenously LPS while continuing the acquisition of the fluorescence decay curves of Ag_2S NPs. Figure 4D shows the time evolution of the fluorescence lifetime of Ag_2S NPs during in vivo experiments. A clear decrease in the fluorescence lifetime is observed to occur after LPS administration. Partial stabilization of the average fluorescence lifetime was observed for post-injection times longer than 50 min. By using the calibration curve of Figure 2F we were able to get the time course of liver temperature after LPS injection (Figure 4E). As it can be observed, during the first 50 min following LPS administration, the temperature of the liver increases monotonously with time, and then it tends to stabilize at longer times. The same trend of initial temperature increment followed by stabilization 50 min after LPS administration was observed probing the rectal temperature (also included in Figure 4E). Further comparison between the curves included in Figure 4E reveals that inflammation causes a larger and faster temperature change in the liver when compared to intracorporeal temperature, being the liver the body location where the temperature increase is originated. In addition, the body core temperature (rectal probe) started rising only 20 min after LPS administration, whereas we detected an immediate increase in liver temperature (directly measured by our Ag_2S NPs). Here, the role of the rectal probe is helping to confirm the temperature change trend taking place inside the animal body, as a whole. The higher and steeper temperature increment in the liver is likely caused by the triggering of the inflammatory process involving pyrogens such as prostaglandin E2, which results in a local increase of the temperature of organs in intimate contact with the peritoneal cavity.[30] This includes the liver, which is postulate here to experience the combination of two inflammation-related processes: increment in both the blood perfusion and the local metabolic activity as a consequence of prostaglandin release.[32]

The inflammation-induced heating curve of the liver provided by Ag_2S NPs can be compared to previously published data also dealing with the thermal response of this organ after LPS administration. Rudaya and co-workers, for instance, monitored the intracorporeal temperature of a mouse after LPS administration (similar dose to the one used here). The intracorporeal temperature was measured by implantation of a temperature transmitter in the peritoneal cavity.[33] They found that the activation of an inflammation process elevated the intraperitoneal temperature by 1.5 °C. It should be noted though that we were able to access the liver temperature by a purely contactless technology whereas Rudaya et al. required the implantation of a temperature transmitter in the peritoneal cavity. Such an aggressive approach compromises the natural thermal response of the individual as it alters blood perfusion, mass and effective thermal conductivity of organs in close proximity to the implant.[34] Our results can also be compared to those recently published by Lu and co-workers, who used hydrogen- sulfide-activatable near-infrared emitting NPs for the detection of liver inflammation. The authors reported liver inflammation 45 min after LPS administration but, unlike in our present study, the time evolution of the process was not investigated.[35]

Lastly, we should point out that the potential of Ag_2S NPs for liver temperature monitoring is not restricted to studies in the framework of inflammatory processes. Indeed, we also tested their suitability for accurate, absolute, and contactless thermal monitoring during laser driven hyperthermia processes (Figure S7, Supporting Information). Results are included in Figure S8 (Supporting Information), and they open the door to future development of fully controlled hyperthermia treatments of liver, where on-the-fly adjustment of the therapeutic parameters (e.g., laser power) could become possible. While acknowledging the enhancement achieved through the approach described in the present work, we also recognize that, if we aim for application in humans in the long-term, the limitations imposed by currently available detection systems will also need to be taken into account. Given the present circumstances, the best-case scenario seems to be the application of luminescent thermometers in human skin, muscles, joints, breast tissue, or the most external parts of the brain.[36] Thus, we believe that studies correlating the presence of incipient diseases in such organs with temperature would certainly benefit from the accuracy provided by lifetime-based luminescence thermometry.

3. Conclusion

This work demonstrates that reliable, accurate, and contactless in vivo thermal monitoring of internal organs can be achieved via lifetime-based thermometry using infrared-emitting Ag_2S nanoparticles. The high brightness of the sonochemically prepared Ag_2S nanoparticles guarantees low-noise fluorescence signal, while their long lifetimes avoid the requirement of using ultrafast lasers for optical excitation. By using lifetime as a thermometric parameter, the thermal readout is unperturbed by the presence of tissue in the optical path between the imaged

region and the detector. We demonstrated how lifetime-based Ag_2S nanothermometers enable accurate (uncertainty below 0.3 °C), real-time monitoring of the liver temperature during an ongoing inflammatory process in small animal models. This demonstration of thermal sensing in a deep organ is remarkable evidence of the potential of lifetime-based luminescence nanothermometry beyond the current state of the art.

The results included in this work clear up the doubts that hovered over the potential of nanothermometry at the preclinical level due to the inevitable spectral distortion caused by photon-tissue interaction. To that end, the use of fluorescence lifetime as thermometric parameter emerges as a viable solution to the issues related to the reliability of luminescence nanothermometry. Hence, we foresee that the development of new lifetime-based thermal nanosensors with improved brightness and longer fluorescence lifetimes will help establishing luminescence nanothermometry as a standard method in preclinical research.

4. Experimental Section

Synthesis of Ag_2S NPs: Ag_2S NPs were synthesized through the thermal decomposition method starting from the precursor silver diethyldithiocarbamate (AgDDTC), previously prepared by the reaction between 0.025 mmol of $AgNO_3$ and 0.025 mmol of NaDDTC, separately pre-dissolved in 200 mL of Milli-Q water.[37] The slowly addition of the NaDDTC solution above the $AgNO_3$ solution produced a yellow precipitate (AgDDTC). The product was filtered under vacuum, dried at 60 °C and stored in a desiccator protected from light for its following use. The production of Ag_2S NPs was carried out by adding 25 mg of AgDDTC (0.1 mmol), 2.5 mL of 1-dodecanethiol (DDT, 10.4 mmol) and 2.5 mL of oleyl amine (OLA, 7.6 mmol) into a two-necked round-bottom flask at room temperature (RT). The mixture was first sonicated under vacuum for 10 min to remove air and rests of water. After that, the mixture was heated up to 185 °C at a heating rate of 20 °C min^{-1} in nitrogen atmosphere under slow magnetic stirring. The reaction was kept for 1 h and subsequently cooled down naturally. The synthesized NPs were destabilized with 10 mL of ethanol and collected by centrifugation at 10 000 g for 10 min; this process was repeated twice. Finally, the NPs pellet was dispersed in $CHCl_3$ at a concentration of 1 mg mL^{-1} and stored at 4 °C for further steps.

Stabilization of the Ag_2S NPs in PBS through PEGylation: The Ag_2S NPs need to be transferred to an aqueous media for their following application. Figure S1 (Supporting information) includes a schematic diagram of functionalization procedure. Their stabilization in PBS was initiated through a ligand exchange reaction between capping agents (DDT and OLA) and 1-mercaptoundecanoic acid (MUA) units, which introduce carboxylic groups on the surface rendering negatively charged nanoparticles and stabilizing colloidally the synthesized nanoparticles. For that, 20 mg (0.1 mmol) of MUA were added to 1 mL of dispersion of Ag_2S NPs in $CHCl_3$ at RT. The reaction was facilitated under sonication for 5 min until the NPs lose their colloidal stability and start to aggregate. The NPs functionalized with MUA were collected via centrifugation at 1000 g for 2 min and dispersed in 1 mL of PBS at pH 7.4. Subsequently, PEGylation via EDC/NHS coupling was carried out with the aim of covering the NPs properly for the in vivo experiments. To do that, 1 mg of PEG-NH_2 (MW = 5 kDa), 0.5 mg of EDC and 0.7 mg of sulfo-NHS were dissolved in 1 mL of PBS containing 1 mg of the previously prepared Ag_2S-MUA NPs. The mixture was gently stirred for 4 h, and after that, the NPs were collected by centrifugation using Amicon centrifugal filters (MWCO = 50 kDa) at 9600 g for 10 min. This washing process was repeated three times and the resulting NPs were finally dispersed in 1 mL of PBS and stored at 4 °C.

Material Characterization: FTIR Measurements: Hydrodynamic diameter and ζ-potential of Ag_2S NPs were measured with a Malvern Nano-ZS. In the first case, the mean diffusion coefficient was derived from the intensity autocorrelation function using cumulant analysis and converted into mean particle size via the Stokes–Einstein equation, whereas ζ-potential measurements were based on the principles of laser Doppler electrophoresis. Infrared spectra were recorded using a Thermo Nicolet IR200 spectrometer with Fourier Transform. Samples were prepared as potassium bromide discs with 2–5% (w/w) of analyte. All the spectra were recorded with 256 scans. Figure S3 (Supporting Information) includes the FTIR spectra of the as synthesized Ag_2S NPs, MUA-functionalized NPs and PEGlyated NPs.

Fluorescence Quantum Yield (QY) measurements: The QY of the Ag_2S NPs was measured with a 6 inch diameter integrating sphere (Labsphere, 4P-GPS-060-SF). The sample cuvette (5 mm path length) was mounted at the center of the sphere. Light from a pigtailed 808 nm laser (Omicrom, BrixX808-2500-HP-FC) was collimated onto the sample with a beam diameter of 2.5 mm. The collected signal was sent to a monochromator (Horiba, iHR320) for wavelength selection and detected with an NIR InGaAs photodetector (Horiba, DSS-IGA020TC).

The QY was calculated by dividing the total number of emitted photons in the emission range (950–1500 nm) by the total number of absorbed photons in the excitation range (800–810 nm). The number of absorbed photons is calculated from the difference between two spectra: the spectrum of the excitation light (808 nm) with the Ag_2S sample, and the spectrum with the PBS reference sample. The number of emitted photons by the Ag_2S sample when irradiated at 808 nm is calculated from the emission spectra. Then, to calculate the QY, all the spectra are corrected by the system response in the emission and the excitation spectral regions using a calibrated halogen lamp (Ocean Optics, HL3-INT-CAL-EXT). QY has been measured for Ag_2S NPs in PBS at 0.5 mg mL^{-1} and with an excitation power of 10 mW.

Animal Handling and LPS Administration: All procedures involving animal experiments were approved by the regional authority for animal experimentation of the Comunidad de Madrid, with an ethical approval number PROEX 221-19 correlated with the proposal entitled "Use of optical nanoparticles for early detection of hepatic alterations induced by acute inflammation or fat diet". Experiments were conducted in agreement with the Universidad Autónoma de Madrid Ethics Committee and in compliance with the European Union directives 63/2010UE and Spanish regulation RD 53/2013. CD1 female mice ($n = 5$) (weight, 30 g; age, 8 weeks old) were employed for the in vivo experiments under isoflurane anesthesia (4% isoflurane 2 L min^{-1} O_2 for induction, 1.5% isoflurane 0.5 L min^{-1} O_2, for maintenance). After the lifetime sensing experiments were complete, euthanasia was performed beheading the animal under 5% of isoflurane inhaled anesthesia. Animals were simultaneously monitored for the recording of body core temperature trough a rectal probe and for liver deep temperature using LNTs. The animals were first monitored to achieve a stable and reproducible temperature of 36.5 °C. For the monitoring of hepatic gene expression of inflammatory markers, the mRNA levels of TNF-α, IL-1β, IL-6, and iNOS were assessed in liver samples from mice intraperitoneally injected with saline (10 mL kg^{-1}; $n = 4$) or with LPS (10 mg kg^{-1}; $n = 4$) 4 h after injection. For that purpose, total RNA was extracted from 100 mg of hepatic tissue using the Tri-Reagent protocol.[1] Afterward, cDNA was synthesized from 1 µg of total RNA, using a high-capacity cDNA reverse transcription kit (Applied Biosystems, Foster City, CA, USA). Relative gene expression was measured by quantitative real-time PCR using assay-on-demand kits (Applied Biosystems, Foster City, CA, USA) for each gene. TaqMan Universal PCR Master Mix (Applied Biosystems, Foster City, CA, USA) was used for amplification in a Step One machine (Applied Biosystems, Foster City, CA, USA). Values were normalized to the housekeeping gene 18S. To determine relative expression levels the ΔCt method was used.[38] For each mouse, average values from saline and LPS injected mice for each gene were statistically compared using unpaired *t*-test. Changes were considered significant when $p < 0.05$.

Acquisition of Decay Curves in In Vivo Conditions: For the acquisition of the fluorescence decay curves of Ag_2S NPs within the liver, we illuminated the anesthetized mouse with 800 nm laser pulses of 10 ns of duration and pulse-to-pulse separation of 0.1 s. This pulse-to-pulse separation was fixed and given by the laser source but had the additional advantage of minimizing thermal loading between consecutive pulses. The spot size during in vivo experiments was set to 0.1 cm^2. The laser fluence was set to 1.5×10^{-2} J cm^{-2}, i.e., below the reported threshold for skin damage under infrared nanosecond laser pulses excitation (≈0.1 J cm^{-2}).[39] The fluorescence generated by the Ag_2S NPs was collected by a set of lenses and spectrally filtered by a monochromator. The decay of the fluorescence intensity generated at 1240 ± 20 nm was finally recorded by an infrared photomultiplier connected to a digital oscilloscope. The average fluorescence lifetime was estimated and translated into temperature units by using the calibration curve (Figure 2F). Further discussion about the data dispersion of lifetime in vivo recording (from fluorescence decay curves) is analyzed in Section S5 (Supporting Information).

Supporting Information

Supporting Information is available from the Wiley Online Library or from the author.

Acknowledgements

Y.S. J.L., and I.Z.-G. contributed equally to this work. This work was supported by the Spanish Ministerio de Ciencia under project PID2019-106211RB-I00 and Ministerio de Economía y Competitividad under project MAT2017-83111R, by the Comunidad Autónoma de Madrid (B2017/BMD-3867 RENIM-CM), and co-financed by the European Structural and Investment fund. Additional funding was provided by the European Union's Horizon 2020 FET Open program (Grant Agreement No. 801305, NanoTBTech), and also by COST action CA17140. Y.S. acknowledges a scholarship from the China Scholarship Council (No. 201806870023). I.Z.-G. thanks UCM-Santander for a predoctoral contract (CT63/19-CT64/19). M.F was funded by a research contract from the Community of Madrid (PEJ-2018-AI/SAL-11315). E.X. is grateful for a Juan de la Cierva Formación scholarship (FJC2018-036734-I). J.L. is grateful for FPI scholarship PID2019-106211RB-100. A. B. acknowledges funding from Comunidad de Madrid through TALENTO grant ref. 2019-T1/IND-14014.

Conflict of Interest

The authors declare no conflict of interest.

Data Availability Statement

The data that support the findings of this study are available from the corresponding author upon reasonable request.

Keywords

inflammation, temperature-dependent fluorescence lifetime, nanothermometry, organ-temperature monitoring, high thermal sensitivity

Received: September 28, 2021
Revised: November 25, 2021
Published online: January 9, 2022

[1] C. L. Tan, Z. A. Knight, *Neuron* **2018**, *98*, 31.
[2] a) M. M. Sajadi, P. A. Mackowiak, in *Mandell, Douglas, and Bennett's Principles and Practice of Infectious Diseases*, 8th ed. (Eds: J. E. Bennett, R. Dolin, M. J. Blaser), **2015**, p. 708; b) H. Wang, M. Kim, K. P. Normoyle, D. Llano, *Front. Neurosci.* **2015**, *9*, 528; c) B. F. Jones, *IEEE Trans. Med. Imaging* **1998**, *17*, 1019; d) C. Stefanadis, L. Diamantopoulos, J. Dernellis, E. Economou, E. Tsiamis, K. Toutouzas, C. Vlachopoulos, P. Toutouzas, *J. Mol. Cell. Cardiol.* **2000**, *32*, 43.
[3] M. Bauer, H. Gerlach, T. Vogelmann, F. Preissing, J. Stiefel, D. Adam, *Crit. Care* **2020**, *24*, 239.
[4] S. Kacmaz, E. Ercelebi, S. Zengin, S. Cindoruk, *Infrared Phys. Technol.* **2017**, *86*, 120.
[5] D. S. Moran, L. Mendal, *Sports Med.* **2002**, *32*, 879.
[6] a) C. D. S. Brites, P. P. Lima, N. J. O. Silva, A. Millan, V. S. Amaral, F. Palacio, L. D. Carlos, *Nanoscale* **2012**, *4*, 4799; b) C. D. S. Brites, S. Balabhadra, L. D. Carlos, *Adv. Opt. Mater.* **2019**, *7*, 1801239; c) D. Jaque, F. Vetrone, *Nanoscale* **2012**, *4*, 4301.
[7] A. Bednarkiewicz, L. Marciniak, L. D. Carlos, D. Jaque, *Nanoscale* **2020**, *12*, 14405.
[8] a) F. Vetrone, R. Naccache, A. Zamarrón, A. Juarranz de la Fuente, F. Sanz-Rodríguez, L. Martinez Maestro, E. Martín Rodriguez, D. Jaque, J. García Solé, J. A. Capobianco, *ACS Nano* **2010**, *4*, 3254; b) J.-M. Yang, H. Yang, L. Lin, *ACS Nano* **2011**, *5*, 5067; c) J. S. Donner, S. A. Thompson, M. P. Kreuzer, G. Baffou, R. Quidant, *Nano Lett.* **2012**, *12*, 2107.
[9] K. Okabe, N. Inada, C. Gota, Y. Harada, T. Funatsu, S. Uchiyama, *Nat. Commun.* **2012**, *3*, 705.
[10] B. del Rosal, E. Ximendes, U. Rocha, D. Jaque, *Adv. Opt. Mater.* **2016**, *5*, 1600508.
[11] B. del Rosal, D. Ruiz, I. Chaves-Coira, B. H. Juárez, L. Monge, G. Hong, N. Fernández, D. Jaque, *Adv. Funct. Mater.* **2018**, *28*, 1806088.
[12] E. C. Ximendes, U. Rocha, B. del Rosal, A. Vaquero, F. Sanz-Rodríguez, L. Monge, F. Ren, F. Vetrone, D. Ma, J. García-Solé, *Adv. Healthcare Mater.* **2017**, *6*, 1601195.
[13] Y. Shen, H. D. A. Santos, E. C. Ximendes, J. Lifante, A. Sanz-Portilla, L. Monge, N. Fernández, I. Chaves-Coira, C. Jacinto, C. D. S. Brites, L. D. Carlos, A. Benayas, M. C. Iglesias-de la Cruz, D. Jaque, *Adv. Funct. Mater.* **2020**, *30*, 2002730.
[14] a) M. Xu, X. Zou, Q. Su, W. Yuan, C. Cao, Q. Wang, X. Zhu, W. Feng, F. Li, *Nat. Commun.* **2018**, *9*, 2698; b) X. Zhu, W. Feng, J. Chang, Y.-W. Tan, J. Li, M. Chen, Y. Sun, F. Li, *Nat. Commun.* **2016**, *7*, 10437.
[15] Y. Shen, J. Lifante, N. Fernández, D. Jaque, E. Ximendes, *ACS Nano* **2020**, *14*, 4122.
[16] L. Labrador-Páez, M. Pedroni, A. Speghini, J. García-Solé, P. Haro-González, D. Jaque, *Nanoscale* **2018**, *10*, 22319.
[17] J. Zhou, B. del Rosal, D. Jaque, S. Uchiyama, D. Jin, *Nat. Methods* **2020**, *17*, 967.
[18] M. Tan, F. Li, N. Cao, H. Li, X. Wang, C. Zhang, D. Jaque, G. Chen, *Small* **2020**, *16*, 2004118.
[19] a) Y. Zhang, G. Hong, Y. Zhang, G. Chen, F. Li, H. Dai, Q. Wang, *ACS Nano* **2012**, *6*, 3695; b) D. Ruiz, B. del Rosal, M. Acebrón, C. Palencia, C. Sun, J. Cabanillas-González, M. López-Haro, A. B. Hungría, D. Jaque, B. H. Juarez, *Adv. Funct. Mater.* **2017**, *27*, 1604629; c) Y. Zhang, Y. Zhang, G. Hong, W. He, K. Zhou, K. Yang, F. Li, G. Chen, Z. Liu, H. Dai, Q. Wang, *Biomaterials* **2013**, *34*, 3639; d) P. Jiang, C.-N. Zhu, Z.-L. Zhang, Z.-Q. Tian, D.-W. Pang, *Biomaterials* **2012**, *33*, 5130; e) Y. Shen, J. Lifante, E. Ximendes, H. D. A. Santos, D. Ruiz, B. H. Juárez, I. Zabala Gutiérrez, V. Torres Vera, J. Rubio Retama, E. Martín Rodríguez, D. H. Ortgies, D. Jaque, A. Benayas, B. del Rosal, *Nanoscale* **2019**, *11*, 19251.
[20] H. Santos, D. Ruiz, G. Lifante, C. Jacinto, B. Juarez, D. Jaque, *Nanoscale* **2017**, *9*, 2505.

[21] a) M. Hashemkhani, G. Demirci, A. Bayir, A. Muti, A. Sennaroğlu, L. M. Hadi, E. Yaghini, M. Loizidou, A. J. MacRobert, H. Y. Acar, *Nanoscale* **2021**, *13*, 14879; b) M. Gao, H. Zhao, Z. Wang, Y. Zhao, X. Zou, L. Sun, *Adv. Powder Technol.* **2021**, *32*, 1972; c) G. Chen, Y. Zhang, C. Li, Q. Wang, in *Near Infrared-Emitting Nanoparticles for Biomedical Applications* (Eds: A. Benayas, E. Hemmer, G. Hong, D. Jaque), Springer International Publishing, Cham, Switzerland **2020**, pp. 279–304; d) A. Bednarkiewicz, J. Drabik, K. Trejgis, D. Jaque, E. Ximendes, L. Marciniak, *Appl. Phys. Rev.* **2021**, *8*, 011317.
[22] S. Kalytchuk, K. Poláková, Y. Wang, J. P. Froning, K. Cepe, A. L. Rogach, R. Zbořil, *ACS Nano* **2017**, *11*, 1432.
[23] P. Haro-González, L. Martínez-Maestro, I. Martín, J. García-Solé, D. Jaque, *Small* **2012**, *8*, 2652.
[24] T. Chihara, M. Umezawa, K. Miyata, S. Sekiyama, N. Hosokawa, K. Okubo, M. Kamimura, K. Soga, *Sci. Rep.* **2019**, *9*, 12806.
[25] a) P. Lai, X. Xu, L. Wang, *J. Biomed. Opt.* **2014**, *19*, 035002; b) L. Cortese, G. L. Presti, M. Pagliazzi, D. Contini, A. D. Mora, A. Pifferi, S. K. V. Sekar, L. Spinelli, P. Taroni, M. Zanoletti, U. M. Weigel, S. de Fraguier, A. Nguyen-Dihn, B. Rosinski, T. Durduran, *Biomed. Opt. Express* **2018**, *9*, 2068.
[26] S. Fantini, D. Hueber, M. A. Franceschini, E. Gratton, W. Rosenfeld, P. G. Stubblefield, D. Maulik, M. R. Stankovic, *Phys. Med. Biol.* **1999**, *44*, 1543.
[27] R. Nachabe, B. Hendriks, A. Desjardins, M. van der Voort, M. van der Mark, H. Sterenborg, *J. Biomed. Opt.* **2010**, *15*, 037015.
[28] J. Lifante, Y. Shen, I. Zabala Gutierrez, I. Rubia-Rodríguez, D. Ortega, N. Fernandez, S. Melle, M. Granado, J. Rubio-Retama, D. Jaque, E. Ximendes, *Adv. Sci.* **2021**, *8*, 2003838.
[29] A. Garami, A. A. Steiner, A. A. Romanovsky, *Handb. Clin. Neurol.* **2018**, *157*, 565.
[30] K. Hamesch, E. Borkham-Kamphorst, P. Strnad, R. Weiskirchen, *Lab. Anim.* **2015**, *49*, 37.
[31] F. E. Maturi, C. D. S. Brites, E. C. Ximendes, C. Mills, B. Olsen, D. Jaque, S. J. L. Ribeiro, L. D. Carlos, *Laser Photonics Rev.***2021**, *15*, 2100301.
[32] E. Ricciotti, G. A. FitzGerald, *Arterioscler., Thromb., Vasc. Biol.* **2011**, *31*, 986.
[33] A. Y. Rudaya, A. A. Steiner, J. R. Robbins, A. S. Dragic, A. A. Romanovsky, *Am. J. Physiol.: Regul., Integr. Comp. Physiol.* **2005**, *289*, R1244.
[34] M. Zaltieri, C. Massaroni, F. M. Cauti, E. Schena, *Sensors* **2021**, *21*, 1453.
[35] Q. Liu, Y. Zhong, Y. Su, L. Zhao, J. Peng, *Nano Lett.* **2021**, *21*, 4606.
[36] E. Ximendes, A. Benayas, D. Jaque, R. Marin, *ACS Nano* **2021**, *15*, 1917.
[37] A. Ortega, Y. Shen, I. Z. Gutierrez, H. D. A. Santos, V. T. Vera, E. Ximendes, G. Villaverde, J. L. Cañabete, C. Gerke, N. Fernandez, O. G. Calderón, S. Melle, J. M. Hueso, D. M. Gonzalez, M. Laurenti, C. Jones, J. M. L. Romero, R. C. Caceres, D. Jaque, J. R. Retama, *ACS Appl. Mater. Interfaces* **2020**, *12*, 12500.
[38] P. Chomczynski, *BioTechniques* **1993**, *15*, 532.
[39] M. DeLisi, A. Peterson, G. Noojin, A. Shingledecker, A. Tijerina, A. Boretsky, M. Schmidt, S. Kumru, R. Thomas, *Proc. SPIE* **2018**, *10492*, 1049207.